HIGHER-ORDER STRUCTURAL CONSTRAINTS
FOR IMPROVED OPTIMIZATION
OF NONUNIFORM HELICAL ANTENNAS

Graeme E. Innes

Private Researcher, Milton, Ontario, Canada

Abstract. *The objective is to improve the linear constraints for optimizing the helical structure (radius and pitch of the conductor winding) of nonuniform helical antennas for desired characteristics such as signal gain or bandwidth. Presented below are equations that allow various higher-order structural constraints to be used in such optimizations. Their efficacy is demonstrated by analogy, using data for a fully optimized Yagi-Uda antenna, before being applied to data available for helical designs. The comparisons confirm the general validity of the higher-order equations to model some of the most advanced antennas produced to date. A simple calculus-of-variations test confirms that an improved optimization is possible by adding curvature terms to previously published linear constraints.*

Key words: *Curvature, Higher-order Constraint, Improved Optimization, Nonuniform Helical Antenna, Simple Test, Structural Constraint*

1. INTRODUCTION

The helical antenna in its most basic configuration consists of a single wire coiled into a helix, mounted with the axis perpendicular to a nearby conducting ground plane, Fig. 1. This design naturally produces circularly polarized radiation, which makes it useful in applications with arbitrary signal polarization such as for satellite and space communication.

For the first three decades following publication of the earliest study in 1947, development of the helical antenna relied on empirical methods using physical prototypes [1,2]. That paradigm shifted in the 1980's with the emergence of numerical simulation tools, such as Numerical Electromagnetics Code (NEC), WIPL-D and MATLAB® [3-5], that can solve the nonlinear sets of equations describing antenna operation. These enable evaluation and improvement of a design before constructing the physical antenna.

By the 1990's, numerical optimization for characteristics such as gain or bandwidth was routinely carried out for some antenna types, such as the well-known Yagi-Uda design [6,7]. It was not until a decade later that computing resources were equal to the

task of handling the complexities involved with optimizing the most basic helical antenna. The first such study for helices with an infinite ground plane and single copper winding of constant radius r and pitch p was published in 2006 [8]. The study considered various antenna lengths and several wire sizes wound in a hexagonal helix formation, which is amenable to software modelling the conductor as a series of linear segments.

Yet one more decade passed before adequate computing resources became available to enable landmark studies of nonuniform helical antennas with various wire properties. Two exhaustive global optimizations of a 2x2 array of such antennas were carried out by [9] with the constraints of linearly varying helix radius r and helix pitch p with respect to the axial distance z. In this case, the number of variables to be optimized for a single helical antenna is 4, consisting of r_1 and p_1 at the helix base ($z = 0$) and r_2 and p_2 at the top ($z = L$), Fig. 2. The imposed linear form leads to a single-exponential relation for the location z at each turn of the helix n. The antenna length was fixed at $L = 2.5\lambda$, where λ is the wavelength of the nominal design frequency. A subsequent large-scale study [10] considered various antenna lengths, along with different wire conductivities and sizes.

By relaxing the linear constraints to allow parabolic variation of r and p with respect to z, a double-exponential relation for z in terms of n results. By analogy, this is shown to yield a superior optimization result approaching that already achieved for Yagi-Uda antennas, where data for element-by-element simulations are readily available.

The equivalent feat in the case of a helical antenna would be a turn-by-turn optimization, which currently can be prohibitive in terms of computational effort. For a single helix, the number of variables to be optimized would rise dramatically to $2n$, where solutions of interest might lie in the range $20 < n < 50$. A large-scale study involving just 7 variables required millions of individual simulations or solver calls [10] to yield on the order of thousands of optimized designs, highlighting the need for efficient constraints using as few variables as possible.
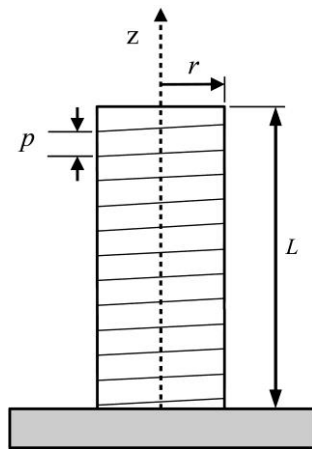
Fig. 1 Profile view of a uniform helical antenna of length L with a winding of constant radius r and pitch p.
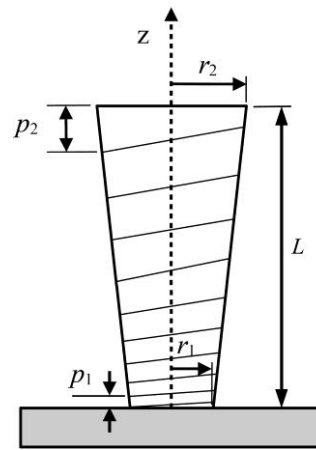
Fig. 2 Profile view of a nonuniform helical antenna of length L with a winding of linearly varying radius r and pitch p.

By adding just two more variables to be optimized, an improvement over the linearly constrained optimization may be obtained. Specifically, these are the coefficients k_r and k_p introduced below that control the magnitude of the curvature terms and which are shown in Figs 3 and 4. The necessary parabolic forms for r and p are presented and the double-exponential relation is derived for the z locations of each turn n. Limits for values of the curvature coefficients k are evaluated before illustrating the accuracy of the parabolic equations using a set of optimized Yagi-Uda data. The Yagi structure is nominally comparable to the helical antenna and study of the optimized shape offers a means to improve the helical design.

An alternative bi-linear form is compared briefly and several power law forms presented that, in combination with the parabolic forms, show even further flexibility in modelling nonuniform antenna structures. The results are then extended to exponential forms. The accuracy is demonstrated by comparison with data from the literature and the Internet for a variety of helical and circularly polarized Yagi-Uda types of design, as well as an alternative pair of trigonometric forms. Expressing these in non-dimensional form simplifies presentation of the mathematics.

Finally, a simple calculus-of-variations test is presented that shows higher-order constraints will generally give an improved optimization over the linear constraints, especially for shorter antennas where $L \leq 2\lambda$.
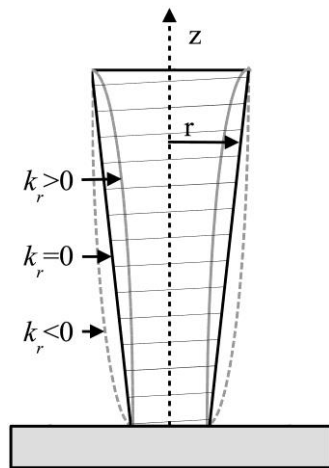
Fig. 3 Effect of radius curvature on the helix profile: $k_r > 0$ is concave and $k_r < 0$ is convex.
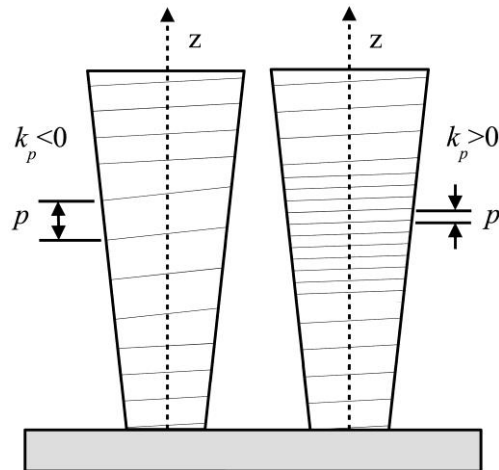
Fig. 4 Effect of pitch curvature on the helix winding: $k_p < 0$ increases pitch and $k_p > 0$ decreases pitch.

2. PARABOLIC FORM

2.1. Parabolic constraints

The second-order polynomial relations for helix radius r and pitch p may be written in non-dimensional form:

$$R = k_r Z^2 + (a_r - k_r)Z + 1 \tag{1}$$

$$P = k_p Z^2 + (a_p - k_p)Z + 1 = \frac{dZ}{dN} \tag{2}$$

where the coefficients k_r and k_p control the magnitude of each Z^2 term (curvature term) and the following non-dimensional groups are defined: $R = r/r_1$ is the radius of the helix winding, $P = p/p_1$ is the pitch of the winding, $Z = z/L$ is the axial distance, $a_r = (r_2-r_1)/r_1$ is the radius taper, $a_p = (p_2-p_1)/p_1$ is the pitch taper and $N = n(p_1/L)$ is the reduced turn number.

The pitch angle [10] is sometimes used as an alternative to the helix pitch, with the definition $\varphi = \tan^{-1}(p/2\pi r) \approx p/2\pi r$ radians, or $\varphi \approx 90p/\pi^2 r$ degrees. This approximation is accurate to within 1 percent for $\varphi < 9.86$ degrees and to within 2 percent for $\varphi < 13.87$ degrees. Substitution into Eq. (2) allows convenient comparison of the two systems to the same order of accuracy, which may be acceptable for many practical cases.

Eqs (1) and (2) reduce to the linear cases for $k_r = k_p = 0$. The radius curvature coefficient $k_r > 0$ for concave helix profiles and $k_r < 0$ for convex profiles, Fig. 3, and the pitch curvature coefficient k_p imposes a comparable pattern onto the helix winding, Fig. 4. The limits for values of the coefficients are explored in the next Subsection.

Eq. (2) may be rearranged, integrated and the boundary condition $N = 0$ at $Z = 0$ applied to yield:

$$N = \frac{1}{k_p(Q_2 - Q_1)} \ln\left(\frac{Z/Q_2 - 1}{Z/Q_1 - 1} \right) \tag{3}$$

where, defining $b = (a_p - k_p)/2k_p$, the two quadratic root quantities are:

$$Q_1 = -b - \sqrt{b^2 - 1/k_p} \tag{4}$$

$$Q_2 = -b + \sqrt{b^2 - 1/k_p} \tag{5}$$

Taking $Z = 1$ allows calculation of the total number of turns $n_{tot} = N_{tot}(L/p_1)$ of the helix winding. Rearranging for Z, a double-exponential relation in terms of N results:

$$Z = \frac{\exp[k_p(Q_2 - Q_1)N] - 1}{(1/Q_1)\exp[k_p(Q_2 - Q_1)N] - (1/Q_2)} \tag{6}$$

which allows the axial position of each turn to be determined. Eqs (3) to (6) break down for $k_p = 0$, in which case they become:

$$N = \frac{1}{a_p}\ln(a_p Z + 1) \tag{7}$$

$$Z = \frac{1}{a_p}\exp[(a_p N) - 1] \tag{8}$$

For $r_1 = r_2$, the helix profile reduces to a constant radius cylinder ($a_r = k_r = 0$). For $p_1 = p_2$, the pitch taper $a_p = 0$ and the helix winding has a constant pitch $p = L/n_{tot} = z/n$. In that case, Eqs (7) and (8) reduce to $N = Z$ and $Z = N$.

2.2. Limits for values of the coefficients k

Eqs (1) and (2) are formulated to produce curves that pass through specified end points at $Z = 0$ and $Z = 1$. However, for certain values of the coefficient k, they are capable of generating negative values of the helix radius and pitch in the axial range of interest $0 \leq Z \leq 1$. These correspond to physically impossible situations, so it is necessary to limit the range of values that k may assume. The effect of the radial curvature coefficient is explored first and the results extended to the pitch curvature.

Fig. 5 shows several possible helix profiles that may be produced by Eq (1). The non-dimensional helix radius R exhibits a minimum for $k_r > 0$ (concave profile) and a maximum for $k_r < 0$ (convex profile). These occur where the slope $dR/dZ = 2k_rZ + (a_r - k_r) = 0$ and thus a formula for k_r may be written:

$$k_r = \frac{a_r}{1 - 2Z} \tag{9}$$

The curves for $k_r = +a_r$ and $k_r = -a_r$ have zero slope at one of the helix endpoints. These curves bracket the already optimized linear helix profile [9,10] and the optimized parabolic shape will likely lie nearby, in the range $-a_r \leq k_r \leq a_r$. It is noted that Eq. (9) has a discontinuity for $Z = 0.5$ and can only have physical meaning if $a_r = 0$ also, i.e., the helix radius has no linear taper component in this case.

However, if $k_r > 0$ is too large, Eq. (1) will generate negative values for the helix radius. The constraint condition may be written as $R \geq 0$ in the range $0 \leq Z \leq 1$. By rearranging Eq. (9) we obtain the axial position of the parabola minimum, namely $Z = -(a_r - k_r)/2k_r$, and substituting this into Eq. (1) gives the condition:

$$-(k_r - q_1)(k_r - q_2) \geq 0 \tag{10}$$

where the quadratic roots are:
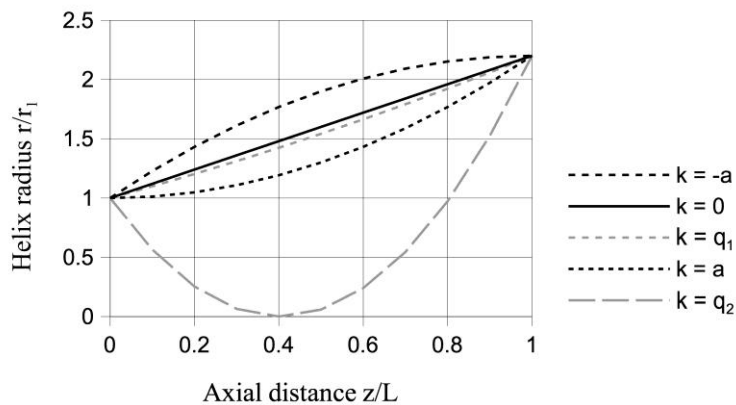
Fig. 5 Helix profiles for $a_r = 1.2$ over a range of radius curvature coefficients k_r.

$$q_1 = (a_r + 2) - 2\sqrt{a_r + 1} \tag{11}$$

$$q_2 = (a_r + 2) + 2\sqrt{a_r + 1} \tag{12}$$

From Fig. 5, it may be seen that a minimum in the range $0 \leq Z \leq 1$ only occurs for $k_r = q_2$, thus Eq. (1) generates positive values when:

$$k_r < q_2 \tag{13}$$

It is noted that, by definition $a_r = (r_2 - r_1)/r_1$ and because r_2 must not be negative, the radius taper is confined to the range $-1 \leq a_r \leq \infty$. This avoids the generation of complex values by Eqs (11) and (12).

Regarding the pitch curvature, by substituting a_p for a_r in Eqs (11) and (12), the comparable condition for positive pitch values for Eq. (2) is:

$$k_p < q_2 \tag{14}$$

Furthermore, the pitch curvature coefficient $k_p < 0$ cannot be too negative or it will reduce the number of turns in Eq. (3) to less than a desired value, typically $n = 4$. An iterative method with $Z = 1$, $n = 4$ and fixed values of a_p was used to determine the k_p values for this constraint. For the linearly optimized case [9] $p_1/L = 17\text{mm}/750\text{mm}$, the resulting curve for k_p versus a_p is plotted in Fig. 6. This reveals the lower limit for k_p is orders of magnitude outside of the range of interest here.

The nonlinear equations presented elsewhere in this paper also require an iterative solution to determine limits for values of the curvature coefficients. A practical step in an optimization algorithm might be simply to check for negative values of r and p every time the structural dimensions are recalculated.

2.3. Optimized Yagi-Uda test case

The Yagi-Uda antenna has a nominally comparable structure to the helical antenna; hence by studying optimized versions of the former, it may be possible to improve the design of the latter. The data for a 15-element Yagi-Uda antenna optimized for gain were produced with a method-of-moments solution [11] embodied in a Java applet [6,7] and the results posted on the Internet [12]. Curve-fitting these data with the form of equations for the helical antenna, an analogy may be developed.
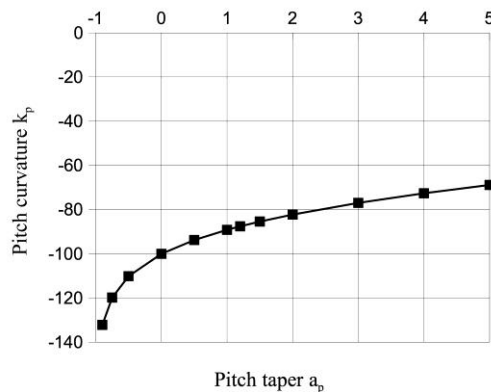
Fig. 6 Variation of k_p with a_p, where $p_1/L = 0.0227$, to produce a helix with $n = 4$ turns.

Table 1 lists the equivalent parameters used when comparing the two antenna designs. The two structures are also depicted in Fig. 7. The Yagi-Uda design features a series of discrete linear elements positioned perpendicular to the z axis, while the helical design features a conductive ground plane at $z = 0$ plus a single wire coiled along the z axis.

For consistency, the Yagi-Uda elements are numbered here as 0-14 and not 1-15 as conventionally done, so that the reflectors count as 0 in both antenna designs. Thus $n_{tot} = 14$ and the normalized element number $\mathbf{N} = n/n_{tot}$, corresponds to the helical normalized turn number $\mathbf{N}$, where $0 \leq \mathbf{N} \leq 1$.

The optimized Yagi-Uda antenna here consists of 14 parasitic or passive elements and one driven element (#1). Data points for this element and the reflector (#0) were included in the calculations for the best-fit coefficients although they do not always fit well with the overall pattern of the helical equations.

Table 1 Equivalent non-dimensional parameters for Helical and Yagi-Uda antennas.

Helix parameter	Yagi parameter
Axial distance from reflector, Z	Axial distance from reflector, Z
Helix radius for 1 turn, R	Element length, R
Helix pitch for 1 turn, P	Element spacing, P
Normalized turn number, $\mathbf{N}$	Normalized element number, $\mathbf{N}$
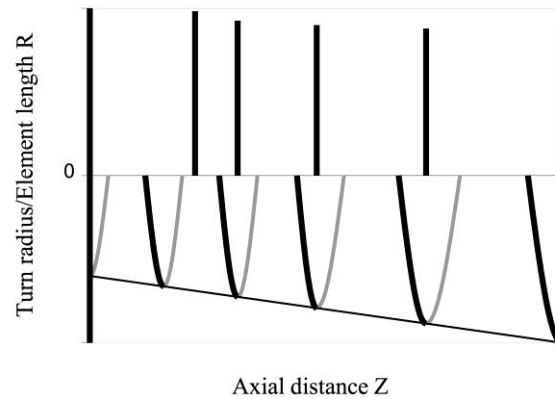
Fig. 7 Comparison of antenna structures: Yagi-Uda (upper half) and nonuniform helix profile (lower half).

Fig. 8 shows element length R versus axial distance, while Fig. 9 shows the element spacing P, derived from linear interpolation of the data, versus axial distance. A least-squares method [13] was adapted to minimize the error of the second-order curve-fits.

The parabolic curves (solid lines) show a superior fit to these data compared with the linear counterparts (dashed lines). This indicates that, had the Yagi optimization proceeded with constraints of the parabolic form, a better approximation to the true optimized data would have emerged compared with the linear constraints.

By analogy, using the parabolic constraints for optimizing the helical antenna should result in a better approximation to the true optimized data than the linear constraints.

2.4. Comparison with bi-linear form

The linear constraints could be taken one step further and a bi-linear form used instead of the continuously variable parabolic Eqs (1) and (2). Figs 10 and 11 show such an arrangement obtains an agreement with the Yagi-Uda data that rivals that of the parabolic curves.

However, the use of piecewise linear segments has the cost of optimizing the range of each segment. Thus in general, 4 new variables would be added: a middle radius r_m and middle pitch p_m and their respective axial locations L_{rm} and L_{pm}. Even after simplifying with $L_{rm} = L_{pm}$, 3 new variables would be added, compared with just the 2 curvature coefficients of the parabolic forms.
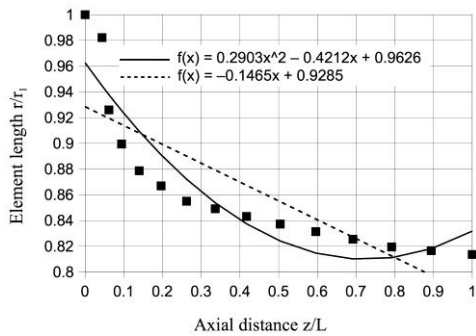
Fig. 8 Optimized Yagi element length R versus axial distance Z.
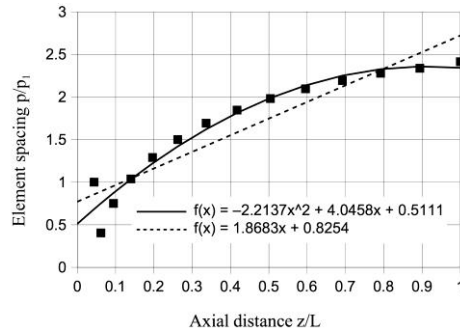
Fig. 9 Optimized Yagi element spacing P versus axial distance Z.
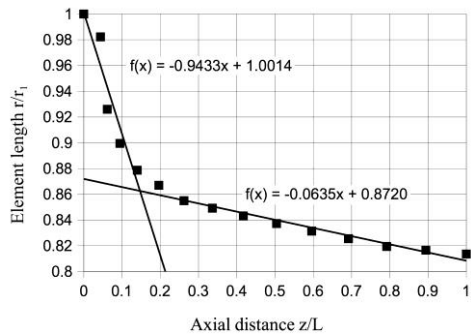
Fig. 10 Optimized Yagi element length R versus axial distance Z with a bi-linear curve-fit.
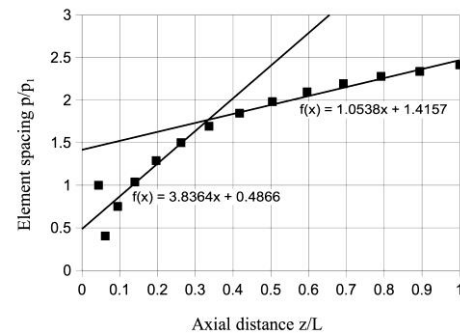
Fig. 11 Optimized Yagi element spacing P versus axial distance Z with a bi-linear curve-fit.

3. POWER-LAW FORMS

3.1. Direct power-law curve-fits

Further improvement in accuracy is obtained by applying a power-law formula directly to the optimized Yagi-Uda data, Figs 12 and 13, particularly for the sharply flared profile at one end of the element array.

The element length taper and element spacing taper are indicated by the dashed lines in each Figure, which correspond to the helical tapers a_r and a_p. The helical power-law form, including linear tapers, is presented in the following Subsection.

3.2. Power-law-plus-linear equations

The close approximation of the parabolic curve-fit in Fig. 9, along with the improved power-law approximation of Fig. 12, suggests that the power-law form may be used in combination with the parabolic form. This combination of equations is desirable since the power-law form adds one more variable to be optimized: the power-law exponent C.

However, the "raw" power-law curve-fit in Fig. 12 has a negative exponent, which means Z^C would tend to infinity, not zero, as $Z \to 0$. This difficulty is overcome with the formulations presented below.

Thus, three new scenarios result:

(a) The pitch is kept as parabolic in terms of Z, Eq. (2), while the radius R is modified to allow an arbitrary exponent $C > 0$, producing a power-law-plus-linear form:

$$R = k_r Z^C + (a_r - k_r)Z + 1 \tag{15}$$

Eq. (15) reduces to Eq. (1) when $C = 2$.
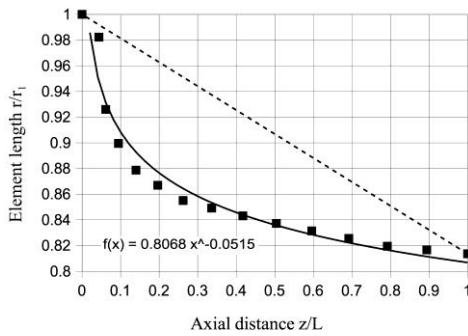
Fig. 12 Optimized Yagi element length R versus axial distance Z with a power-law curve-fit.
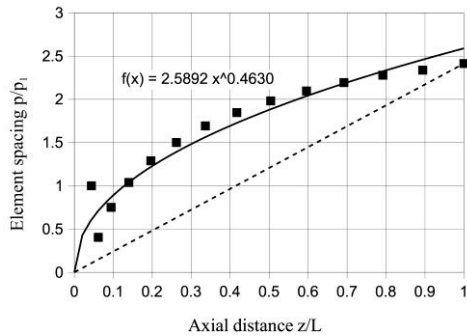
Fig. 13 Optimized Yagi element spacing P versus axial distance Z with a power-law curve-fit.

(b) The radius is kept as parabolic in terms of Z, Eq. (1), while the pitch P is modified to allow an arbitrary exponent $D > 0$, producing a power-law-plus-linear form:

$$P = k_p Z^D + (a_p - k_p)Z + 1 = \frac{dZ}{dN} \tag{16}$$

Eq. (16) reduces to Eq. (2) when $D = 2$. However, when rearranging and integrating to obtain $N(Z)$ the analysis is cumbersome, involving an infinite series expansion. Alternatively, $N(Z)$ and $Z(N)$ may be determined by numerical methods.

(c) Both the pitch and radius may have power-law forms in terms of Z, but the same cumbersome integration problem of (b) remains.

3.3. N-form of power-law-plus-linear equations

The analytical difficulty may be avoided by re-stating the non-dimensional radius and pitch directly in terms of the normalized turn number $\mathbf{N} = N/N_{tot} = n/n_{tot}$:

$$R = k_r \mathbf{N}^C + (a_r - k_r)\mathbf{N} + 1 \tag{17}$$

$$P = k_p \mathbf{N}^D + (a_p - k_p)\mathbf{N} + 1 = \frac{1}{N_{tot}}\frac{dZ}{d\mathbf{N}} \tag{18}$$

where $0 \leq \mathbf{N} \leq 1$ and N_{tot} is the reduced turn number at $Z = 1$. Eq. (18) may be rearranged, integrated and the boundary condition applied $N = 0$ at $Z = 0$ to give:

$$Z = N_{tot}\left(\frac{k_p}{D+1}\mathbf{N}^{D+1} + \frac{a_p - k_p}{2}\mathbf{N}^2 + \mathbf{N}\right) \tag{19}$$

and N_{tot} is easily found:

$$N_{tot} = \left(\frac{k_p}{D+1} + \frac{a_p - k_p}{2} + 1\right)^{-1} \tag{20}$$

Eq. (19) may be used iteratively to solve for $N = N(Z)$.

Fig. 14 shows a curve-fit using the form of Eq. (17) with an R versus $\mathbf{N}$ plot of the optimized Yagi-Uda data. The problem of the negative exponent of Fig. 12 is overcome. It also shows that plotting against the normalized element number $\mathbf{N}$ produces a gentler flare than plotting against Z. The rms error in element length is 0.728 percent with the power-law-plus-linear form.

Fig. 15 shows a curve-fit using the form of Eq. (19) with a Z versus $\mathbf{N}$ plot of the optimized Yagi-Uda data. The linearly interpolated pitch values shown in Figs 9, 11 and 13 are replaced by a smoothed $Z(\mathbf{N})$ curve, from which a smoothed pitch $P = dZ/dN$ curve may be derived.
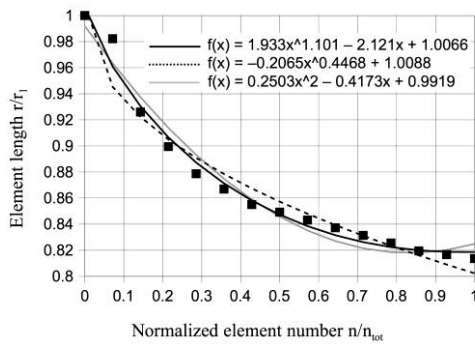
Fig. 14 Optimized Yagi element length R versus normalized element number $\mathbf{N}$ with power-law based curve-fits.
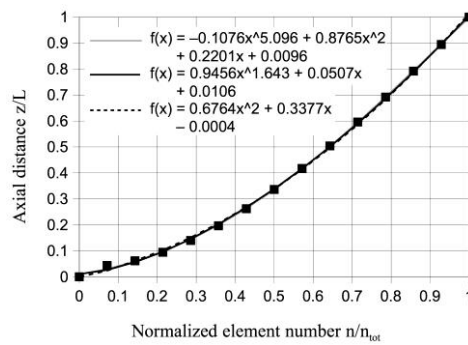
Fig. 15 Optimized Yagi axial distance Z versus normalized element number $\mathbf{N}$ with power-law based curve-fits.

3.4. Simplified power-law forms

The power-law-plus-linear curve in Fig. 15 is virtually identical to that generated by the power-law-plus-parabola form Eq. (19). This suggests the pitch curvature coefficient $k_p = a_p$ for this data set, which reduces the number of variables by one.

Furthermore, the nature of the $Z(\mathbf{N})$ curve in Fig. 15 allows the simplification $k_p = 0$ with $a_p \neq 0$. The resulting simple parabolic form of Eq. (19) is scarcely visible as a dashed curve, revealing the accuracy is also quite good for this data set. This would eliminate yet again one more variable, since Eq. (18) would be reduced to the linear form.

The equivalent simplification for the radius curvature coefficient $k_r = a_r$ was applied in Fig. 14 to produce a power-law-plus-constant form (dashed curve) with a somewhat poorer fit. Again, this reduces the number of variables by one while delivering better capability to model profiles with a sharp flare at one end compared with the parabolic form (gray curve). The best-fit parabola gives a much closer approximation to the data when plotted against $\mathbf{N}$, compared with plotting against Z (Fig. 8).

4. EXPONENTIAL FORMS

4.1. Exponential-plus-linear equations

An exponential term may be substituted for the power-law term in Eqs (15) and (16). For this purpose, it is convenient to define a normalized exponential function for each equation:

$$E_r(Z) = \frac{e^{CZ} - 1}{e^C - 1} \quad \text{(radius)} \tag{21}$$

$$E_p(Z) = \frac{e^{DZ} - 1}{e^D - 1} \quad \text{(pitch)} \tag{22}$$

where $0 \leq E \leq 1$ in the range $0 \leq Z \leq 1$ and C and D are the exponential constants to be optimized. These constants may be positive or negative, unlike for the power-law form where they are constrained to be positive only. The normalized form allows generation of curves that pass through specified points at $Z = 0$ and $Z = 1$. Thus, the radius and pitch constraints become:

$$R = k_r E_r(Z) + (a_r - k_r)Z + 1 \tag{23}$$

$$P = k_p E_p(Z) + (a_p - k_p)Z + 1 = \frac{dZ}{dN} \tag{24}$$

4.2. N-form of exponential-plus-linear equations

As with the power-law-plus-linear form, the analytical difficulty in integrating the rearranged Eq. (24) to obtain $Z(N)$ and $N(Z)$ may be avoided by re-stating the non-dimensional radius and pitch directly in terms of the normalized turn number $\mathbf{N}$:

$$R = k_r E_r(\mathbf{N}) + (a_r - k_r)\mathbf{N} + 1 \tag{25}$$

$$P = k_p E_p(\mathbf{N}) + (a_p - k_p)\mathbf{N} + 1 = \frac{1}{N_{tot}} \frac{dZ}{d\mathbf{N}} \qquad (26)$$

This may be rearranged, integrated and the boundary condition applied $N = 0$ at $Z = 0$ to give:

$$Z = N_{tot}\left[k_p\left(\frac{E_p(\mathbf{N})}{D} - \frac{\mathbf{N}}{e^D - 1}\right) + \frac{a_p - k_p}{2}\mathbf{N}^2 + \mathbf{N}\right] \qquad (27)$$

and N_{tot} is readily found:

$$N_{tot} = \left[k_p\left(\frac{1}{D} - \frac{1}{e^D - 1}\right) + \frac{a_p - k_p}{2} + 1\right]^{-1} \qquad (28)$$

Figs 16 and 17 reveal this form obtains a comparably close fit to the optimized Yagi-Uda data as the power-law-plus-linear form. The rms error in element length is 0.588 percent with the exponential-plus-linear form, Fig. 16.

It is noted that Eq. (27) does not reduce to Eq. (8), as these expressions were formulated differently.

4.3. Simplified exponential forms

As in Subsection 3.3, applying the simplification $k_r = a_r$ to the radius constraint allows the number of variables to be reduced by one. Fig. 16 reveals the exponential-plus-constant form (dashed curve) is noticeably better than the power-law-plus-constant form of Fig. 14. It would also be preferred over the less accurate parabolic form (gray curve). All three of these forms involve 3 variables to be optimized.

The exponential-plus-linear curve in Fig. 17 for the element spacing data is virtually identical to that generated by the exponential-plus-parabola form of Eq. (27). Again, this suggests the pitch curvature coefficient $k_p = a_p$ for this data set, which reduces the number of variables by one.
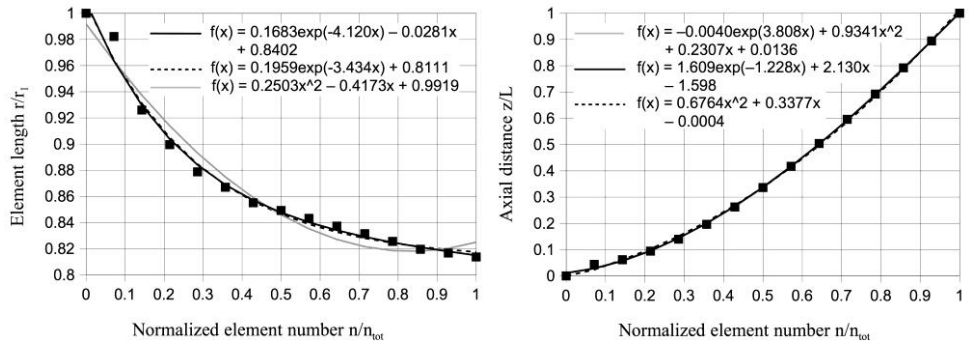
Fig. 16 Optimized Yagi element length R versus normalized element number N with exponential based curve-fits.

Fig. 17 Optimized Yagi axial distance Z versus normalized element number **N** with exponential based curve-fits.

Furthermore, the simplification $k_p = 0$ with $a_p \neq 0$ may be used, yielding the same parabola (dashed curve) as in Fig. 15. This choice reduces Eq. (26) to the linear form, which has only 2 variables to be optimized.

Further subtle improvements to the fit may be obtained with yet higher forms, but at the cost of adding more variables to be optimized. Thus it appears a satisfactory level of efficiency may be achieved, whereby a near-perfect approximation to the true optimized data set results from optimizing as few as 5 variables: r_1, r_2, p_1, p_2 and C, with $k_r = a_r = (r_2/r_1-1)$ and $k_p = 0$ ($a_p \neq 0$).

5. COMPARISON WITH CIRCULARLY POLARIZED DESIGNS

5.1. Types of design

The combined parabolic, power-law-plus-linear and exponential-plus-linear forms offer the capability of closely approximating the structures of a variety of antenna designs that feature circularly polarized operation. These include, with the aid of external circuitry, a circularly polarized Yagi hybrid [14] and a cubical quad [15,16] (square-loop-element Yagi). Designs with inherent circular polarization include helices with tapered ends [17], a bifilar Archimedean-spiral-over-conical-helix design [18] and concave and convex helix profiles [19].

The latter published two normalized trigonometric forms, which may be closely approximated by the forms presented above. Table 2 lists sample curve-fit equivalents for the trigonometric forms.

Figs 18-26 illustrate curve-fits of the data sets. The following patterns occur that demonstrate the capabilities of the higher-order forms:

a) negative slope transitioning to level curve
b) level curve transitioning to negative slope
c) positive slope transitioning to level curve
d) level curve transitioning to positive slope
e) nearly linear curves.

The accuracy of each curve-fit is stated for each Subsection.
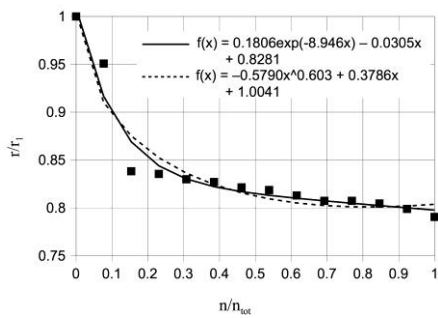
Fig. 18 Element length R versus normalized element number **N** for "Quagi" antenna [14].
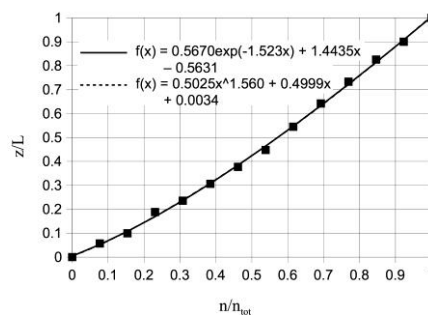
Fig. 19 Axial distance Z versus normalized element number **N** for "Quagi" antenna [14].

5.2. Yagi hybrid

The 435 MHz circularly polarized "Quagi" or Yagi hybrid [14] featured here has two identical orthogonal arrays of Yagi-Uda elements. However, elements #0 and #1 are square loops and are included in Fig. 18 using wire lengths for half of a loop. This hybrid antenna is thus part Yagi-Uda and part cubical quad (presented below). Figs 18 and 19 show $R(\mathbf{N})$ and $Z(\mathbf{N})$ curves similar to the Yagi-Uda test case presented in the previous Sections.

The rms errors for Fig. 18 are 1.651% for the power-law form and 1.313% for the exponential form. The rms errors for Fig. 19 are 0.944% for the power-law form and 0.913% for the exponential form.

5.3. Cubical quad

Figs 20 and 21 show the structural data for the cubical quad [16] design, which features square-loop elements arranged in a Yagi-Uda type array. Only parabolic curve-fits were suitable, as the best-fit exponential and power-law forms exhibited highly linear behaviours for this data set.

For the $Z(\mathbf{N})$ data of Fig. 21, the best-fit exponential-plus-linear and power-law-plus-linear forms each exhibited a singularity for $\mathbf{N} \rightarrow 0$ ($\exp(-\infty\mathbf{N})$ and $\mathbf{N}^0$, respectively). This simply means a mathematically exact curve-fit was possible, but with a discontinuous curve.

The rms error for Fig. 20 is 0.111% and for Fig. 21 is 0.556%.

5.4. Tapered helix

Fig. 22 shows the R profile data for an 18-turn tapered helix [17] and Fig. 23 shows the R profile data for a 9-turn tapered helix. The helix pitch was constant for these two antennas. These Figures highlight the capability of the higher-order equations to handle a sharp change in the helix profile.

The rms errors for Fig. 22 are 1.470% for the power-law form and 1.534% for the exponential form. The rms errors for Fig. 23 are 1.149% for the power-law form and 1.234% for the exponential form.
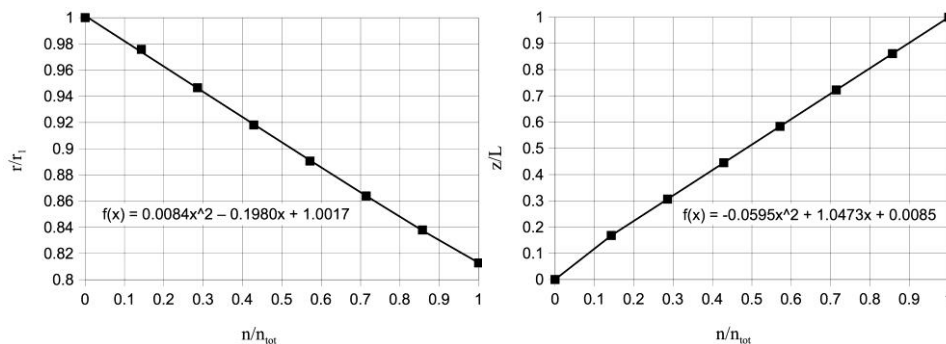
Fig. 20 Element length R versus normalized element number $\mathbf{N}$ for the cubical quad antenna [16].

Fig. 21 Axial distance Z versus normalized element number $\mathbf{N}$ for the cubical quad antenna [16].
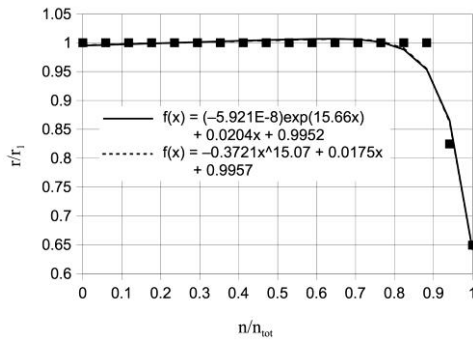
Fig. 22 Helix radius *R* vs. normalized turn number **N** for an 18-turn tapered helix [17].
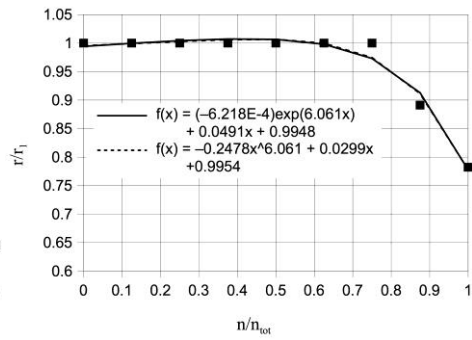
Fig. 23 Helix radius *R* versus normalized turn number **N** for a 9-turn tapered helix [17].
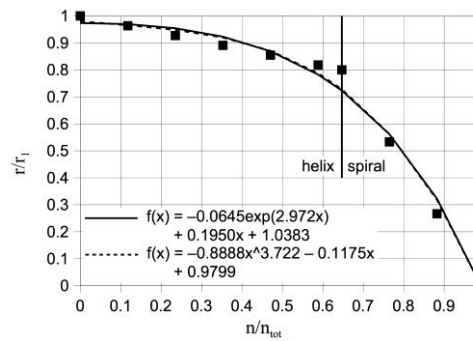
Fig. 24 Helix radius *R* versus normalized turn number **N** for the Archimedean-spiral-over-conical-helix design [18].
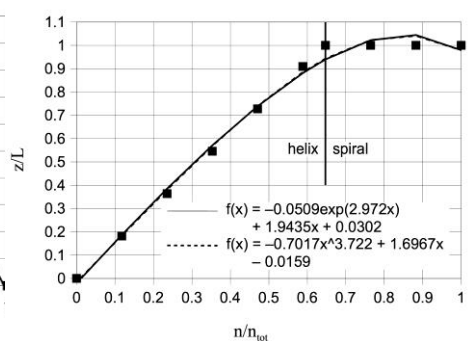
Fig. 25 Axial distance *Z* vs. normalized turn number **N** for the Archimedean-spiral-over-conical-helix design [18].

5.5. Archimedean-spiral-over-conical-helix

The spiral-over-helix [18] design featured here has two identical interlaced windings, rotated 180 degrees apart about the vertical axis *Z*. Only one winding is depicted in Figs 24 and 25. The winding starts at *Z* = 0 as a conical helix and joins the flat Archimedean spiral at *Z* = 1. The conical helix has 5.5 turns and the spiral an undeclared number of turns – at least 3 turns were assumed here.

The capability of describing both sections of the winding with a single higher-order equation is illustrated by this example. It is also noted that since *Z* = 1 for all the spiral turns, the pitch *P* of the flat spiral conductors is given by *dR/dN* instead of the helical *dZ/dN*.

The rms errors for Fig. 24 are 3.509% for the power-law form and 3.801% for the exponential form. The rms errors for Fig. 25 are 2.770% for the power-law form and 3.001% for the exponential form.

5.6. Two trigonometric forms

Two higher-order equations presented for concave and convex helix profiles [19] are in normalized trigonometric form, Eqs (29) and (30):

$$T_1 = 1 - \alpha \tan^{-1} \left[(1-Z) \tan \left(\frac{1}{\alpha} \right) \right] \quad \text{(concave)} \tag{29}$$

$$T_2 = 1 - \left[\tan \left(\frac{1-Z}{\alpha} \right) \right] \bigg/ \tan \left(\frac{1}{\alpha} \right) \quad \text{(convex)} \tag{30}$$

where $T = r/r_2$ (with $r_1 = 0$) and $0 \leq T \leq 1$ over the range $0 \leq Z \leq 1$. The variable to be optimized is $2/\pi < \alpha < \infty$. These are complementary equations with the property of being symmetrical about the line $T = Z$, Fig. 26. This may be shown by rearranging the form of $T(Z)$ to obtain $Z(T)$ in the complementary form, and vice versa. The normalized trigonometric forms are slightly more cumbersome than the forms presented above, since separate equations must be used for the concave and convex cases.

When approximating Eqs (29) and (30) with the power-law and exponential-based forms, sets of data points (Z, T) were first generated and then the curve-fitting process applied. The data points for Eq. (29) were chosen as the intersections between the curve and a family of lines radiating from the point $(Z, T) = (0, 1)$, generated by:

$$T_1 = 1 - Z \cot q \tag{31}$$

where the angle θ was varied in 5-degree increments over the range $0 \leq \theta \leq 90$ degrees. This arrangement produced a relatively uniform distribution of points over the length of each curve. The complementary sets of data for Eq. (30) were generated using Z values equal to the T_1 values from the data sets for Eq. (29).

Table 2 gives examples of the best-fit coefficients for comparable exponential-plus-linear and power-law-plus-linear forms. Fig. 26 illustrates the difference between these curve-fits and the data points.

In Fig. 26, the exponential-plus-linear form (solid curves) was typically better than the power-law-plus-linear form (dashed curves) in approximating the trigonometric form. The overall fit as measured by the difference ΔT_{rms} was better for the concave curves (lower right area) than for the convex curves (upper left). From a practical perspective, where an agreement to within 1 or 2 percent may be acceptable, the choice of normalized form would be a matter of user preference.
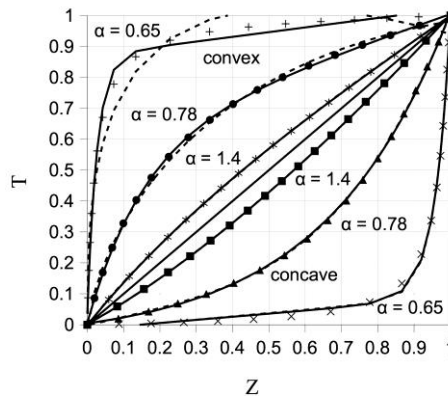
Fig. 26 Trigonometric helix profile T versus axial distance Z for several concave and convex helices [19].

Table 2 Curve-fits of trigonometric data in Fig. 26 using exponential and power-law forms.

α Eq. (29)	Best-fit exponential-plus-linear and power-law- plus-linear forms, plotted in Fig. 26.	ΔT_{rms} (%)
0.65	f(x) = (3.053E-11)exp(24.12x) – 0.1007x– 0.0145	1.080
0.65	f(x) = 0.9050x^23.79 + 0.1071x – 0.0160	1.212
0.78	f(x) = 0.05719exp(2.924x) – 0.0018x – 0.0530	0.428
0.78	f(x) = 0.7419x^3.651 + 0.2666x – 0.0016	0.266
1.4	f(x) = 1.1551exp(-0.8804x) + 1.6767x – 1.1539	0.083
1.4	f(x) = 0.3819x^1.701 + 0.6193x – 0.0014	0.115
Eq. (30)		
0.65	f(x) = –0.8330exp(-36.805x) + 0.1525x + 0.8699	2.250
0.65	f(x) = 1.9899x^0.3352 – 0.9871x – 0.0625	5.457
0.78	f(x) = –0.5892exp(-6.383x) + 0.4096x+ 0.5961	0.356
0.78	f(x) = 3.5057x^0.7709 – 2.5082x – 0.0156	1.122
1.4	f(x) = –0.2506exp(-2.746x) + 0.7652x+ 0.2502	0.028
1.4	f(x) = –1.0416x^1.213 + 2.0405x – 0.0019	0.154

6. SIMPLE TEST OF IMPROVED OPTIMIZATION

An individual optimized helical antenna [9,10] required substantial computational effort to arrive at the structure giving the best signal gain. Without performing any further computation, it may be demonstrated using a calculus-of-variations method that adding curvature terms to the published linear constraints can give improved optimizations.

Fig. 27b shows an end-on view and a profile view of the first 3 turns of a linearly constrained square-helix based on the design of [9,10], with comparison views of a concave version (Fig. 27a) and a convex version (Fig. 27c) generated by the higher-order constraints. A monotonic increase in radius per turn is shown. The helix end points are the same for all three examples.

These views emphasize the helix radius, since the conclusion of Subsection 4.3 suggested that adding curvature to the radius constraint would give the most efficient improvement. The precise form of the higher-order constraint is immaterial, as indicated at the conclusion of Subsection 5.6, for a structural accuracy on the order of 1 or 2 percent.

Assuming the same number of turns n, the same overall helix length L and identical radius and pitch values at $z = 0$ and $z = L$, the concave version has a shorter wire length than the linearly varying helix, while the convex version has a longer wire length. Helix profiles with either a "waist" or "bulge", Fig. 5, could also be considered as they may also have longer or shorter wire lengths.

Thus, when optimizing for signal gain, one of two possible scenarios will generally occur:
(a) the gain increases with an infinitesimal decrease in wire length, or
(b) the gain increases with an infinitesimal increase in wire length.

For scenario (a), a concave helix would have shorter wire length and would thus exhibit superior gain over the linearly varying helix. For scenario (b), the longer wire length of a convex helix would give superior performance compared with the linearly varying helix.

For either scenario, there would exist a better-performing helix generated by the higher-order constraints. Actual effect of the radius curvature on performance will be complicated, but it is demonstrated clearly that an improved optimization is generally possible.
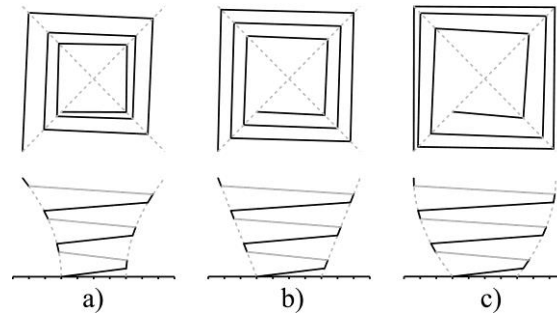
Fig. 27 Overhead views and profile views of square helix windings: a) concave, b) linear and c) convex. The dashed gray lines indicate the physical support structure. The solid gray lines are hidden portions of the winding.

In a simulation with curved helix profiles [19], a concave profile strongly flared at the top ($z = L$) proved best when optimizing for bandwidth with a relatively short helix ($n \approx$ 6). Similarly, the analogy with the Yagi-Uda antenna optimized for gain would also predict a profile with $k_r \approx a_r$ for the optimized helical antenna. The generally positive linear tapers for the optimizations of [9,10] would suggest any concave flare should typically occur at the top of the helix for a longer antenna.

A preliminary survey [10] indicated that nonlinear helix profiles provide little to no improvement in gain for antenna lengths in the range $2\lambda \leq L \leq 10\lambda$. This may be explained using the geometries of the antennas in [9,10]. For a given design frequency, the helix radius is confined to a relatively narrow range of values regardless of antenna length. Thus, the longer the antenna, the more slender it is and the more it resembles a uniform helix.

Conversely, the shorter the antenna, the more conical or curved the profile will appear. Such a pronounced nonlinear shape would therefore be expected to have a greater influence on the electromagnetic properties of the helix, where $L \leq 2\lambda$.

7. Conclusions

7.1. improved structural constraints

Two parabolic relations are proposed to improve the optimizations for helical antennas, compared with the previously published optimizations using linear constraints. By analogy using optimized Yagi-Uda antenna data, a better approximation to the true optimized data may be seen by the use of parabolas. These generally also have an advantage in efficiency over bi-linear forms by adding fewer variables to be optimized.

Also with reference to the optimized Yagi-Uda data, power-law-plus-linear and exponential-plus-linear curve-fits were found to be even more accurate. The number of variables to be optimized is the same as the parabolic form if the radius or pitch curvature coefficient is taken as equal to the linear taper: $k = a$. A further reduction of one variable may be possible with the pitch equations by taking $k_p = 0$ with $a_p \neq 0$, while still retaining good accuracy.

Comparison with data for a variety of antenna designs and with an alternative pair of trigonometric forms confirms the general validity of these mathematical relations in

specifying structural dimensions and positioning of array elements and helical windings. Current helical antenna designs are often limited to constant or linear structural constraints for convenience of manufacture, whereas higher-order constraints enable optimized designs closer to what the laws of physics will allow.

This last point was demonstrated in Section 6, indicating improvement is generally possible by adding curvature terms to the linear structural constraints, especially for helices where $L \leq 2\lambda$. All the foregoing considerations suggest these higher-order equations are immediately capable of delivering improved results when used as constraints in optimization algorithms.

The various parabolic, power-law-plus-linear and exponential-plus-linear equations presented above are summarized in Table 3. There are 36 possible pairings of the 6 pitch equations with the 6 radius equations, not counting simplified versions. The accuracy generally increases as the number of variables to be optimized increases. The linear forms ($k = 0$) have 2 variables each.

Table 3 Summary of higher-order structural constraints for the helix radius and pitch.

Radius Equations	Pitch Equations
Forms with 3 variables	Forms with 3 variables
$R=R(Z)$ parabolic, Eq. (1)	$P=P(Z)$ parabolic, Eq. (2)
	$N=N(Z)$ Eq. (3), $Z=Z(N)$ Eq. (6)
$R=R(N)$ parabolic, Eq. (17), C=2	$P=P(N)$ parabolic, Eq. (18), D=2
	$N=N(Z)$ and $Z=Z(N)$ via Eq. (19), D=2
Forms with 4 variables	Forms with 4 variables
$R=R(Z)$ power-law, Eq. (15)	$P=P(Z)$ power-law, Eq. (16)
	$N=N(Z)$ and $Z=Z(N)$ numerically
$R=R(Z)$ exponential, Eq. (23)	$P = P(Z)$ exponential, Eq. (24)
	$N=N(Z)$ and $Z=Z(N)$ numerically
$R=R(\mathbf{N})$ power-law, Eq. (17)	$P=P(N)$ power-law, Eq. (18)
	$N=N(Z)$ and $Z=Z(N)$ via Eq. (19)
$R=R(\mathbf{N})$ exponential, Eq. (25)	$P=P(N)$ exponential, Eq. (26)
	$N=N(Z)$ and $Z=Z(N)$ via Eq. (27)

7.2. Further refinements

The application of the higher-order equations to optimize the conductor dimensions is left as a future exercise. Published studies commonly use uniform-thickness wires with circular cross-section, although conductive strips oriented either axially (tapes [20]) or radially ("slinky" coils [17]) are reported. The variation of wire cross-sectional radius or strip width would then be included in the overall optimization process.

Optimum selection of a uniform wire thickness has already been considered elsewhere [8,10]. Optimization of the Archimedean spiral antenna [18] included a linear variation in the width of the flat spiral conductors. Adding extra dimensions, a finely coiled form has been superimposed onto the main helix winding [19] using the same the two trigonometric forms as for the main helix. The higher-order constraints presented here could be used as alternative forms to optimize both the fine structure and the main structure.

An important point may be made regarding the "out-of-place" Yagi-Uda elements #0 and #1. Since these exceptions occur for a fully optimized antenna, the analogy with helical antenna optimization suggests the first turn $n = 1$ should have its own variables r and p to be optimized. This might also be the case if an impedance-matching transformer [21] is included in the optimization.

The radius equations presented here assume a relatively simple variation of the helix profile, although a more complicated tapered-helix-on-tapered-helix design with constant pitch has been published [17]. Each tapered helix profile would normally be approximated by a single radius equation from Table 3; hence the double tapered-helix profile must be handled by an equation of yet higher-order.

As more powerful computing resources become available, the structural constraints may be relaxed further to allow forms such as exponential-plus-parabola, plus-cubic-polynomial, plus-quartic, etc., or a two-exponential-plus-linear form, etc. With the increased number of variables to be optimized, more exotic forms of structural constraint may also be found to be efficient, such as Chebyshev polynomials [22] or Catmull-Rom nonlinear splines [23].

Since refinement of the helical winding of the antenna is now approaching a limit, optimizations must be extended to include other structures simultaneously, namely the reflector [24], multi-filar windings with dielectric cores [25,26], antenna arrays and feed impedance-matching components [9].

REFERENCES

[1] J.D. Kraus, "Helical Beam Antennas," *Electronics*, vol. 20, pp. 109–111, April 1947.

[2] J.L. Wong and H.E. King, "Empirical Helix Antenna Design," *Antenna and Propagation Society International Symposium*, vol. 20, pp. 366–369, 1982.

[3] G. Burke and A. Poggio, "NEC Part I: Program Description – Theory", *Technical report*, Lawrence Livermore Laboratory, January 1981.

[4] WIPL-D historical benchmarks from 1980 to the present.

[5] Mathworks factsheet citing the initial release of MATLAB® in 1984

[6] K. Schmidt, Java applet source, 1998.

[7] K. Schmidt, Yagi Modeller notes.

[8] A.R. Djordjević, A.G. Zajić, M.M. Ilić and G.L. Stüber, "Optimization of Helical Antennas", *IEEE Antennas and Propagation Magazine*, vol. 48, no. 6, pp. 107–115, Dec. 2006.

[9] J.L. Dinkić, D.I. Olćan, A.R. Djordjević and A.G. Zajić, "High-Gain Quad Array of Nonuniform Helical Antennas", *Int'l J. Antennas and Propagation*, Article ID 8421809, 12 pp., March 2019.

[10] J. Dinkić, D. Olćan, A. Djordjević and A. Zajić, "Design and Optimization of Nonuniform Helical Antennas with Linearly Varying Geometrical Parameters", *IEEE Access*, 12 pp., in press.

[11] K. Schmidt, "Simplified mutual impedance of nonplanar skew dipoles", *IEEE Trans. on Antennas and Propagation*, vol. 44, no. 9, pp. 1298–99, 1996.

[12] P.G. Collier, Optimized 15-element Yagi-Uda antenna data.

[13] G.E. Innes, "An Experimental and Theoretical Study of Viscous Lifting in Tribology", *Ph.D. Thesis*, Appendix C, Department of Mechanical Engineering, University of Leeds, Leeds, U.K., 1993.

[14] R. Kalmeijer, "Circularly polarized Quagi antennas for space communications".

[15] W.I. Orr and S.D. Cowan, *All About Cubical Quad Antennas*, 2nd Edn. Radio Publications, Inc., Box 149, Wilton, Conn. 06897, 1970.

[16] Cubical quad antenna data, www.basictables.com/amateur-radio/antenna/cubical-quad-antenna

[17] J.L. Wong and H.E. King, "Broadband Quasi-Taper Helical Antennas", *N.T.I.S. Report A046067*, 35 pp., 30 Sept. 1977.

[18] S. Talari, R. Naraiah, and Dr. Ramakrishna, "Tapered Spiral Helix Antenna", *Int'l J. Emerging Tech. Adv. Eng.*, vol. 3, no. 3, pp. 318–25, March 2013.

[19] T. Peng, S. Koulouridis and J.L. Volakis, "Miniaturization of Conical Helical Antenna via Optimized Coiling", *A.C.E.S. J.*, vol. 26, no. 6, pp. 452–58, June 2011.

[20] A.F. Peterson, B.S. Greene and R. Mittra, "Propagation and radiation characteristics of the tape helix with a conducting core and dielectric substrate", *IEEE Trans. on Antennas and Propagation*, vol. 38, no. 4, pp. 578–84, April 1990.

[21] S.V. Savić, M.M. Ilić and A.R. Djordjević, "Design of Internal Wire-Based Impedance Matching of Helical Antennas Using an Equivalent Thin-Wire Model", *Int'l J. Antennas and Propagation*, Article ID 7365793, 5 pp., Dec. 2017.

[22] S. Sharma, R. Rishi and C.C. Tripathi, "Impedance Matching Techniques for Microstrip Patch Antenna", *Indian Journal of Science and Technology*, vol. 10, no. 28, 16 pp., July 2017.

[23] K. Jimisha and S. Kumar, "Optimum design of exponentially varying helical antenna with non uniform pitch profile", International Conference on Communication Computing and Security, *Procedia Technology*, pp. 792–98, June 2012.

[24] A. Đorđević, D. Olćan, M. Ilić and A. Zajić, "Design of Optimal Ground Conductor for the Helical Antenna", In Proceedings of the 50th ETRAN Conference, 3 pp., June 2006.

[25] B. Slade, "The Basics of Quadrifilar Helix Antennas", Technical Publication, Orban Microwave Inc., 1834 N. Alafaya Trl., Suite B, Orlando, FL 32826.

[26] M. Škiljo and Z. Blažević, "Helical Antennas in Satellite Radio Channel". In: Dr. Masoumeh Karimi, editor. *Advances in Satellite Communications*.